Piezo- and Pyroelectric Photothermal Characterization of Polymers as a Function of Temperature

J. MURA,[1] L. C. M. MIRANDA,[1] M. L. BAESSO,[1] A. C. BENTO,[1] A. F. RUBIRA

[1] Departamento de Física, Universidade Estadual de Maringá, 87020-900, Maringá, PR, Brazil

[2] Departamento de Química, Universidade Estadual de Maringá, 87020-900, Maringá, PR, Brazil

Received 28 March 2000; accepted 5 January 2001

ABSTRACT: In this article, piezo- and pyroelectric signals are used for the photothermal characterization of the thermomechanical properties of polymers as a function of temperature. The potentialities of the proposed technique are explored using poly(ethylene terephthalate) as the test sample. The influence of the sample thermal aging on the polymer physical properties is also discussed. The sensitivity of the proposed photothermal technique is tested by comparing its results with complementary dielectric response measurements and X-ray diffraction. © 2001 John Wiley & Sons, Inc. J Appl Polym Sci 82: 2669–2678, 2001

Key words: thermal diffusivity; photothermal techniques; polymer aging; glass transition; poly(ethylene terephtalate)

INTRODUCTION

During the past 15 years, we have witnessed the development and consolidation of a number of techniques for nondestructive characterization of the thermal, optical, and structural properties of materials based on the so-called photothermal techniques. This can be appreciated in some of the existing review articles published in the literature.[1–3] The photothermal techniques are essentially based upon sensing the temperature fluctuation of a given sample due to nonradiative deexcitation processes following the absorption of modulated light.

Apart from having been extensively used in the optical and thermal characterization of a wide spectrum of materials, ranging from semiconductors[4–6] to glasses[7,8] and biological specimens,[9,10] these photothermal techniques have been used in connection with the investigation of different physicochemical properties of polymers,[11–13] and gels and pasty materials,[14] as well as the way in which the processing conditions[14–17] of these materials affect their physical properties.

Despite this growing interest and the importance of the application of these techniques to the polymer research area, so far photothermal measurements have been carried out mostly under near-room temperature conditions. This apparent limitation is essentially dictated by the fact that most of the photothermal polymer measurements reported so far were based upon the use of the so-called photoacoustic technique. In a conventional photoacoustic experimental setup, the sample is enclosed in an air-tight cell and exposed to a chopped light beam. As a result of the periodic heating of the sample due to light absorption, the air pressure inside the cell oscillates at the chop-

Correspondence to: L. C. M. Miranda (miranda@dfi.uem.br).

Contract grant sponsor: CNPq (Brazil).

Journal of Applied Polymer Science, Vol. 82, 2669–2678 (2001)

ping frequency and is detected by a sensitive microphone coupled to one of the cell's walls. The use of an electric microphone is the main reason why applications to polymer research have been restricted to room temperature measurements.

In this article, we discuss the use of an alternative photothermal technique for measurements of thermal properties of polymers as a function of temperature. The proposed technique is based on the use of a piezoelectric transducer consisting of a lead zirconate titanate (PZT) ceramic disk onto which the sample is attached. The whole transducer-sample assembly is mounted on top of a cylindrical heater, so that the temperature can be varied from room temperature up to 180°C. The detection technique is tested using poly(ethylene terephthalate) (PET) as the test sample. Apart from its technological importance, the reason for resorting to PET as test sample is twofold. First, PET is a well-documented material so that one can easily validate the proposed method by comparing our results with the existing literature data. Second, in conventional differential scanning calorimetry (DSC), evaluation of the glass-transition temperature of the amorphous fraction[18] of PET at $\sim$ 67°C is not always well resolved; consequently, the observation of this transition with the proposed methodology would represent a sensitivity test for our technique. Particular emphasis is given to the investigation of how repeated thermal sample cycling affects the polymer thermal properties as well as the glass transition. Finally, to validate and evaluate the sensitivity of our experimental procedure, we have compared our results for the thermophysical properties and the phase-transition observations with those of independent measurements of the dielectric response and X-ray diffraction data.

EXPERIMENTAL

The samples used in this work were taken from a commercial 110-μm-thick PET foil as received from the manufacturer (Rhone-Poulenc). Two distinct sets of samples were prepared. One, for the photothermal measurements, consisting of 12-μm-diameter disk-like samples cut form the original PET foil and coated on one their sides with a roughly 1-μm-thick Bi film. This Bi film was left to undergo further oxidation by exposure to ambient air. In this way we ensured a strong optical absorber for heat deposition on the sample surface. For X-ray diffraction and dielectric measurements, the samples consisted of uncoated 25-mm diameter PET wafers. These samples were cut from two distinct regions of the original PET foil, one from a region in which marks of the calendering process were visually evident, indicating that this region suffered a larger stretching; these samples are designated type A samples. The others are from a highly homogeneous region with no visible traces of calendering; these samples are denoted type B.

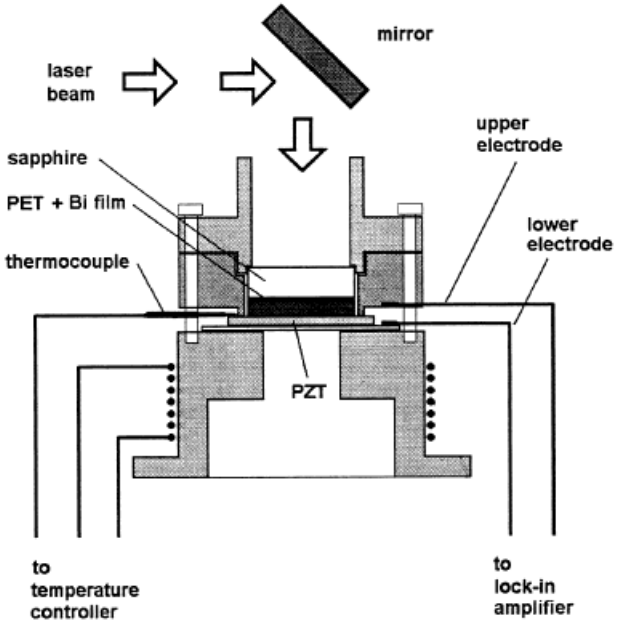

Figure 1 Experimental arrangement for the photothermal characterization of polymer samples as a function of temperature.

The experimental arrangement for the photothermal measurements is schematically shown in Figure 1. It consists of a cylindrical aluminum block, 46-mm outer diameter and 45 mm long. The block has an inner hole of 30-mm diameter and 40 mm long. On the top surface of this base block there is an 8-mm diameter hole, on which the PZT transducer is attached with a thin adhesive layer. The external wall of the base block is wound with heating wire connected to the temperature controller (Novus 1100). A type-T thermocouple, in contact with the PZT ceramic, is fixed on the top cover of the aluminum block and is connected to the control input of the temperature controller. The PZT sensing ceramic consists of a 20-mm diameter wafer, 230 μm thick, deposited on a brass base electrode foil of 27-mm diam-

eter, 230 μm thick. The sample is attached to the PZT detector using a thin layer of thermal paste. The electrical signal from the PZT ceramic is taken from the brass base electrode and an upper electrode screwed to the top cover. This upper electrode consists of an aluminum disk of 46-mm outer diameter with an inner hole of 16-mm diameter, through which the light beam impinges on the Bi-coated surface of the PET sample. At top of the upper electrode, we screw a hollow aluminum guide, with a 12.5-mm-thick sapphire window on its end, whose function is to keep the sample–PZT ceramic assembly mechanically fastened. The measurements were made using the 442-nm line of a 150-mW He–Cd laser (Omnichrome, Series 74), whose output beam was modulated by a mechanical light beam chopper (Stanford Research, model SR540). The output signal from the PZT ceramic was fed into a lock-in amplifier (Stanford Research, model SR530) in which both the amplitude and phase of this input signal were recorded as a function of the modulation frequency, for each temperature of interest, with a range of 20–90°C. All data acquisition was microcomputer controlled. For each sample, we have repeated the temperature cycling three times without removing the sample from the assembly in order to evaluate the influence of sample aging on their thermal properties. During all photothermal measurements, the incident laser power was monitored continuously to warrant that fluctuations of the sample heating were properly taken into account.

The room temperature X-ray diffractograms were recorded using the CuK_α line of a Philips diffractometer (PW1730). The dielectric measurements were carried out using an assembly similar to the photothermal one. An uncoated 25-mm diameter sample wafer is placed on top of a cylindrical aluminum heater which also acted as one of the leads of an LCR impedance meter (Minipa, model MX-801). The heating wires of this cylindrical base electrode were connected to a temperature controller, similar to the photothermal measurement assembly. The upper electrode was a 20-mm diameter tin coated brass disk screwed against the base electrode in such way as to ensure a good mechanical contact with the PET sample sandwiched between these electrodes. For each temperature of interest within the range of 20–90°C we have recorded the capacitance and the dielectric losses at a fixed 1-kHz frequency. As in the photothermal measurements, the effect of sample thermal aging was investigated by repeating the temperature cycling three times without removing the sample from the assembly.

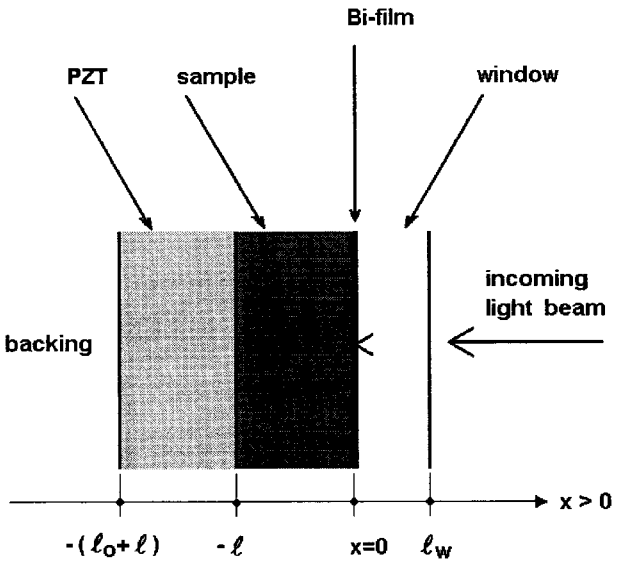

Figure 2 Schematic geometry for the piezo- and pyroelectric photothermal characterization experiment.

PHOTOTHERMAL SIGNAL MODEL

The photothermal signal may be formally described as follows. Consider the geometry shown in Figure 2 representing schematically the physical situation of our experiments. A modulated light beam $I_0e^{j\omega t}$, after passing through a sapphire window, is incident upon the Bi-coated surface of our PET sample of thickness l, at $x = 0$.

We assume that the sample is uniformly illuminated so that a one-dimensional description is adequate. The photothermal signal results from both the piezo- and pyro-electric contributions, which, in turn, depends on the a.c. temperature distribution of the sample-transducer system. Let us denote by α, e, and k the sample thermal diffusivity, effusivity, and conductivity, respectively, and by α_i, e_i, and k_i the corresponding thermal parameters for medium i of thickness l_i. Here, subscripts $i = w$, o, and b denote the window, PZT and backing materials, respectively. The thermal diffusivity and effusivity are related to the thermal conductivity, k, mass density, ρ, and specific heat, c, by $\alpha = k/\rho c$, and $e = (k\rho c)^{1/2}$. Let us also denote by $T(x)e^{j\omega t}$ and $T_i(x)e^{j\omega t}$ the components of the temperature dis-

tribution at the modulation frequency $\omega = 2\pi f$ in the sample and in medium i, respectively. Solving the one-dimensional thermal diffusion equation for the geometry shown in Figure 2, one obtains

$$\langle T\rangle = \frac{\beta' I_0}{l\sigma k\sigma(1+w)}$$

$$\langle T_0\rangle = \frac{2\beta' I_0}{l_0\sigma_0 k_\sigma}\frac{e^{-l\sigma}}{(1+w)(1+p)} \tag{1}$$

for the spatially averaged temperature fluctuations in the sample and PZT, respectively. In Eq. (1), $\beta' = 1 - R_{\text{op}}$ is the surface absorption coefficient, R_{op} is the sample surface optical reflectance, and $w = e_w/e$ and $p = e_0/e$ are the ratios, with respect to the sample, of the thermal effusivities of the window and the PZT, respectively. Parameters w and p represent essentially the thermal impedances of the sample–window and the sample–PZT interfaces. Here, $\sigma = (1+j)(\pi f/\alpha)^{1/2}$ and $\sigma_0 = (1+j)(\pi f/\alpha_0)^{1/2}$ are the complex thermal diffusion coefficients of the sample and the PZT, respectively. In arriving at Eq. (1), we have assumed that, because of the light absorption, all heat is deposited at the sample–window interface at $x = 0$ and that the heat-flux into the surrounding air is negligible. Furthermore, we have also assumed that the sample is thermally thick, namely, that $l\sigma \gg 1$. This assumption is, in general, quite adequate for not so thin polymer samples. For most polymers, the thermal diffusivity is on the order of 0.001 cm^2/s, so the thermal diffusion length, $(\alpha/\pi f)^{1/2}$ will be on the order of 0.0028 cm at a modulation frequency of, say, 40 Hz.

Knowing the temperature distribution in the sample-transducer system, we can then evaluate the photothermal signal by adding up the pyro- and the piezoelectric contributions. An overall view of the formalism describing these two contributions to the photothermal signal can be found in refs. 1–3. For a more detailed discussion on the pyroelectric and piezoelectric detections we refer to works of Coufal[19] and of Jackson and Amer,[20] respectively. The pyroelectric contribution is related to the time derivative of the average temperature fluctuation of the PZT transducer, whereas the piezoelectric one is proportional to the average sample temperature fluctuation. Adding up these two contributions, the photothermal signal S can be written as

$$S = \frac{g l_0 B_{\alpha_T}\beta' I_0}{j\omega l\rho c(1+w)}\,(1 + R\cdot e^{-l\sigma})\cdot e^{j\omega t} \tag{2}$$

where

$$R = \frac{2lP(\alpha_0/\alpha)^{1/2}}{\epsilon g l_0 B_{\alpha_T}(1+p)} \tag{3}$$

In Eqs. (2) and (3), g and P are the PZT piezoelectric and pyroelectric constants, ϵ its dielectric constant, and B and α_T are the sample bulk modulus and thermal expansion coefficient, respectively. In arriving at Eqs. (2) and (3) we have used the fact that the thermal diffusivity is defined as $\alpha = k/\rho c$, where ρ and c are the sample mass density and specific heat, respectively. Performing straightforward calculations, the amplitude, $|S|$, and phase, ϕ, of the photothermal signal, $S = |S|e^{j(\omega t - \phi)}$, can be written as:

$$|S| = \frac{A}{f}\,[1 + 2R\cdot e^{-z}\cos(z) + R^2 e^{-2z}]^{1/2}$$

$$\phi = \frac{\pi}{2} + \tan^{-1}\left[\frac{R\cdot e^{-z}\sin(z)}{1 + R\cdot e^{-z}\cos(z)}\right] \tag{4}$$

where $z = a\sqrt{f}$, $a = l(\pi/\alpha)^{1/2}$, and $A = g l_0 B_{\alpha_T}\beta' I_0/2\pi l\rho c(1+w)$.

Equation (4) describes the modulation frequency dependence of the photothermal signal for our experimental configuration. Parameter a depends essentially on the sample thermal diffusivity, whereas R measures the relative strength of the pyro- and the piezoelectric contributions to the signal buildup. Using the definitions of the thermal diffusivity and effusivity, we can express ρc as $\rho c = e/\sqrt{\alpha}$. Furthermore, noting that for most polymers[18] the thermal effusivity is of the order of 0.1 W $s^{1/2}/cm^2K$, whereas for sapphire,[21] $e = 1.19$ W $s^{1/2}/cm^2K$ that is $e_w \gg e$, we can then approximate $(1 + w)$ by w in the above expression for A. Performing these substitutions in the expression for A, the product $A\cdot a$ can be written as

$$Aa = \frac{g l_0 B\beta' I_0}{2e_w\sqrt{\pi}}\,\alpha_T \tag{5}$$

In the above, the product $A\cdot a$ is essentially proportional to the sample thermal expansion coefficient. We shall call it in what follows a dimen-

sionless thermal expansion coefficient and it will be denoted for short as χ_T. Figure 3 shows the predicted modulation frequency dependence of

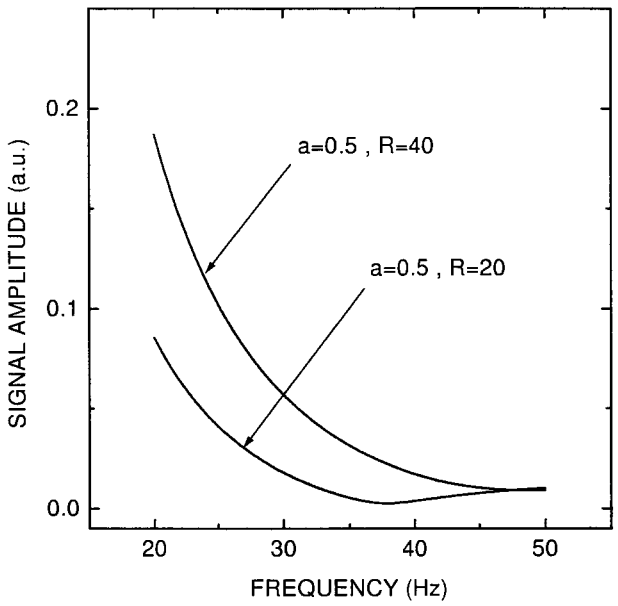

(a)

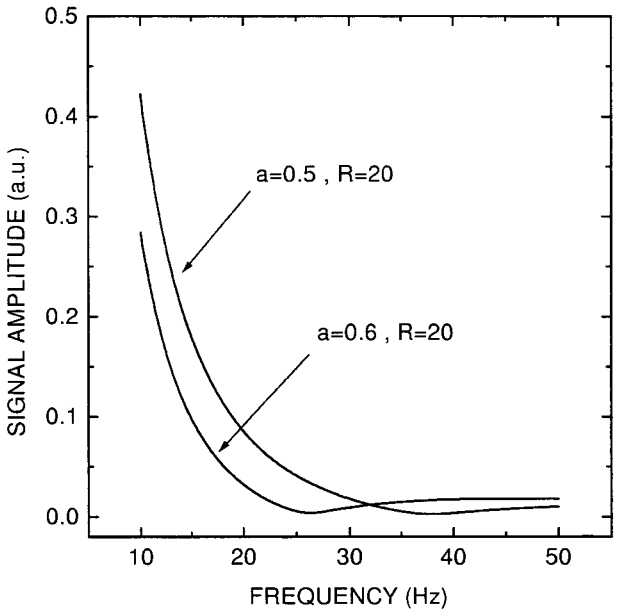

(b)

Figure 3 Frequency dependence of the photothermal signal amplitude, as given by Eq. (4) of the text, for $A = 1$, exhibiting the effect (a) of varying the parameter R, for $a = 0.5$, and the effect (b) of varying the parameter a, for $R = 20$. The parameters in these figures have the same meaning as defined in Eq. (4) of the text.

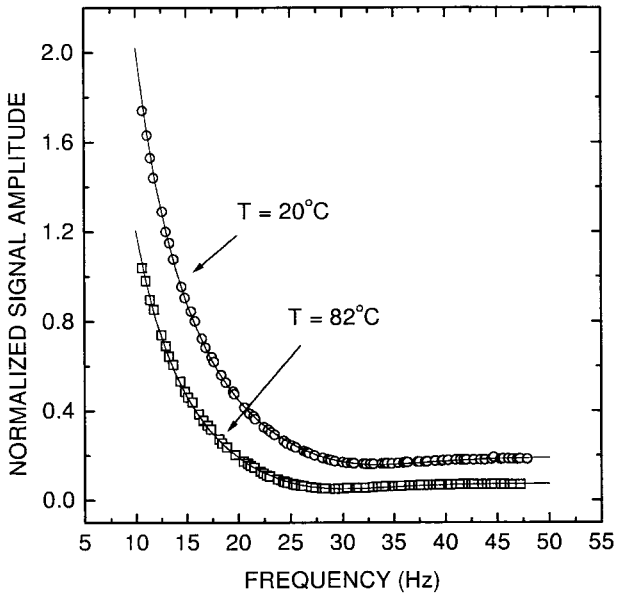

Figure 4 Experimental data for the modulation frequency dependence of the photothermal signal amplitude, normalized to the incident laser power, for a type A poly(ethylene terephthalate) sample at 20°C and 82°C during its first thermal cycling. The solid curves represent the result of the data fitting to Eq. (4) of the text.

the photothermal signal amplitude for different values of a and R, keeping the value of A equal to unity. The curves in Figure 3 differ considerably from the usual exponential decay characteristic[1–3] of the conventional rear-illumination photoacoustic measurement of the thermal diffusivity. Instead, they reflect the competition between the pyro- and the piezoelectric contributions, brought into play by the parameters a and R.

RESULTS AND DISCUSSION

The first set of photothermal measurements we have conducted was carried out on type A samples. Figure 4 shows a typical modulation frequency dependence of the amplitude of the PZT signal for a type A PET sample at 20 and 82°C, during its first thermal cycling, normalized to the incident laser power. The solid line in this figure represents the result of the corresponding data fitting to Eq. (4), in which we have left A, a, and R as adjustable parameters. From the values of a thus obtained, we have calculated the sample thermal diffusivity at each temperature setting.

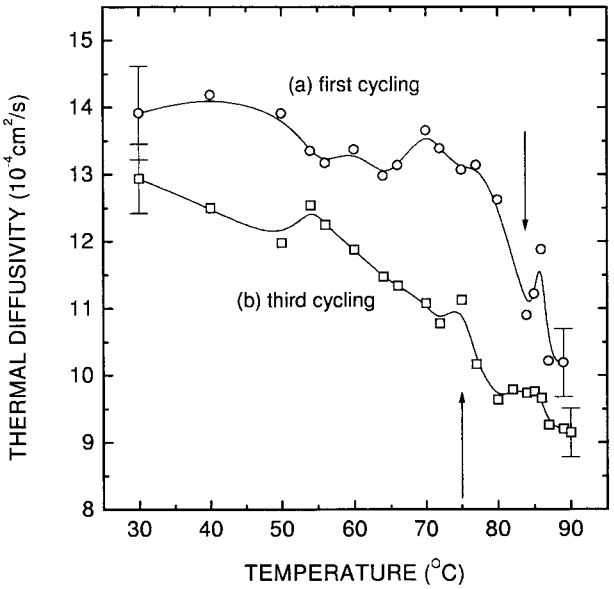

Figure 5 Thermal diffusivity of a type A PET sample as a function of temperature, as obtained from the data fitting procedure for two different sample thermal cycles. The errors bars, corresponding to an average 5% error, are indicated at the beginning and end of the experimental curve for each thermal cycling. The arrows in this figure indicate the glass transition temperature as sensed by the present thermal diffusivity measurements.

The same procedure was carried out for the sequential thermal cycling we have submitted each sample. The results we obtained for the thermal diffusivity of type A samples are shown in Figure 5. Two main features require our attention. First, the thermal diffusivity decreased on increasing the number of thermal cycles to which the sample was submitted. That is, the sample aged with the temperature cycling. The other interesting aspect concerns the peaks the thermal diffusivity curves exhibits at high temperatures. In the first thermal cycling, the thermal diffusivity exhibit a relatively sharp peak at $\sim$ 85°C and a broad jump at $\sim$ 68°C. In contrast, at the third thermal cycling, the sample exhibited a sharp peak at $\sim$ 72°C and a broad one at $\sim$ 84°C. We attribute these peaks of the thermal diffusivity as a manifestation of the glass transition in our PET samples. In fact, according to the literature data,[18] crystalline poly(ethylene terephthalate) exhibits a glass transition at a temperature of 81°C, whereas for amorphous PET the glass transition occurs around 67°C. The combination of this literature information with the results shown in Figure 5 that the sharp peak of α in the first cycling was around 85°C and that, at the third cycling, the main peak was at 72°C, suggests us that the thermal diffusivity data is reflecting the fact that, on subjecting the sample to a thermal cycling above the crystalline glass transition temperature, the sample undergoes an amorphization process. That is, it increases its amorphous fraction. This tentative interpretation of the aging effect exhibited by the thermal diffusivity data was also confirmed by the data of the dimensionless thermal expansion coefficient parameter, $\chi_T = A \cdot \alpha$, as a function of the temperature (Fig. 6). It follows from Figure 6 that, during the first cycling, the parameter χ_T exhibited a sharp peak around 85°C, whereas at the third cycling the more pronounced peak, although broadened, was seen in the neighborhood of 70°C. These results indicate that the proposed photothermal detection is, in principle, capable of not only measuring the thermal diffusivity of a polymer sample as a function of temperature, but it is also sensitive to changes in the sample crystallinity induced by aging (thermal cycling) processes.

To check further the above interpretation of the photothermal results we have next carried out

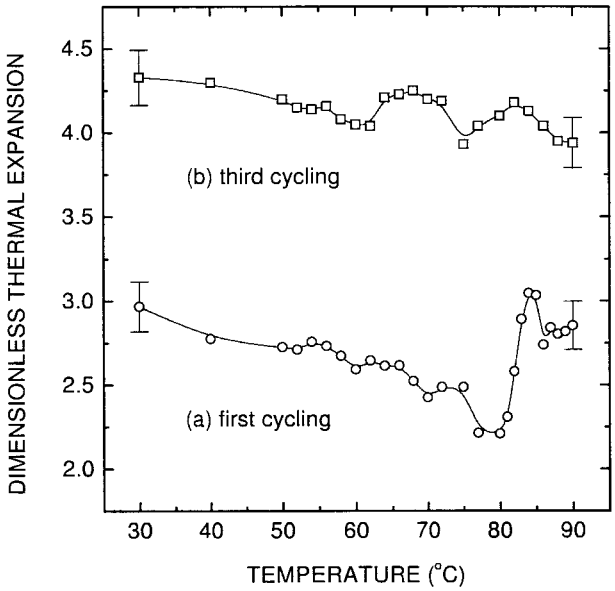

Figure 6 Dimensionless thermal expansion parameter, χ_T, as defined by Eq. (5) of the text for a type A PET sample as a function of temperature, as obtained from the data fitting procedure for two different sample thermal cycles. The errors bars, corresponding to an average 4.5% error, are indicated at the beginning and end of the experimental curve for each thermal cycle.

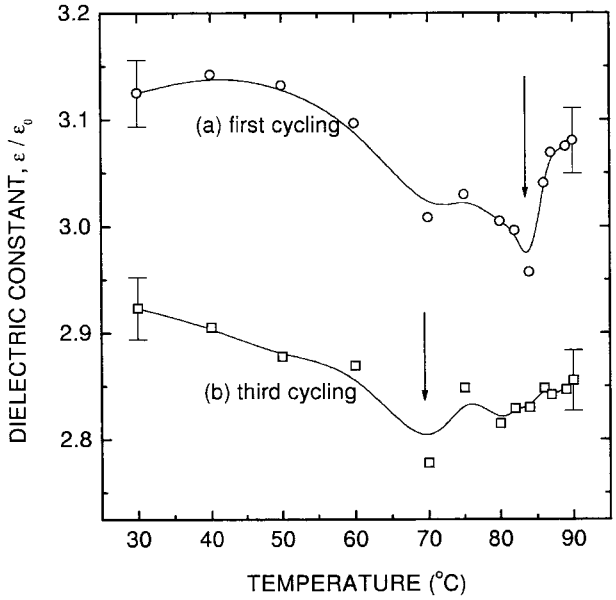

Figure 7 Dielectric constant, ϵ/ϵ_0, of a type A sample as a function of temperature for two different thermal cycles. The errors bars are indicated at the beginning and end of the experimental curve for each thermal cycle. Arrows indicate the glass-transition temperature.

independent measurements of the dielectric response and X-ray diffraction on the same type of samples. Figure 7 summarizes the results we got for the dielectric constant, ϵ/ϵ_0, of type *A* PET sample, as a function of temperature for the first and the third temperature cycles. In the first thermal cycling, the dielectric constant started at a value on the order of 3.1, in good agreement with the literature data.[18] On increasing the temperature, it eventually passed through a relatively sharp minimum around 84°C. At the third cycling, the dielectric constant started, near room temperature, at a lower initial value, as compared with that of the first cycling, and exhibited a minimum at ~ 70°C. That is, in the first thermal cycling, the marked minimum of ϵ/ϵ_0 occurred around the glass transition temperature of the crystalline fraction. After undergoing two consecutive thermal cyclings, the minimum of ϵ/ϵ_0 shifted toward the position of the glass transition temperature characteristic of amorphous PET.

Figure 8(a) and 8(b) shows the X-ray diffractograms corresponding to two distinct type A PET samples. One, corresponding to an uncycled type A sample, namely [Fig. 8(a)], and another one [cf. Fig. 8(b)], corresponding to a type A sample after undergoing the thermal cycling for three times. The main difference between these two diffractograms is that the one corresponding to the thermally cycled sample exhibited broader peaks as compared to that of the uncycled sample, especially at 18° and 23°, corresponding to the characteristic peaks of crystalline PET.[21] The broadening of the X-ray diffraction peaks at 18° and 23°, as a function of the thermal cycling the sam-

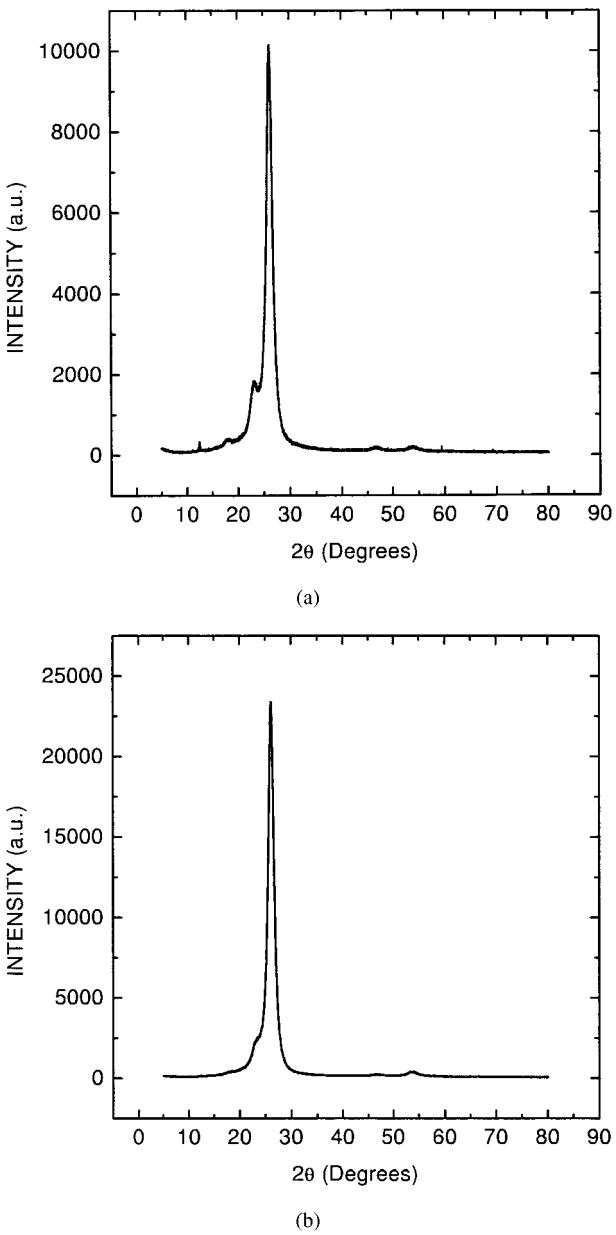

Figure 8 X-ray diffractograms for of a type A sample corresponding to the uncycled situation (a), and after undergoing thermal cycling three times (b).

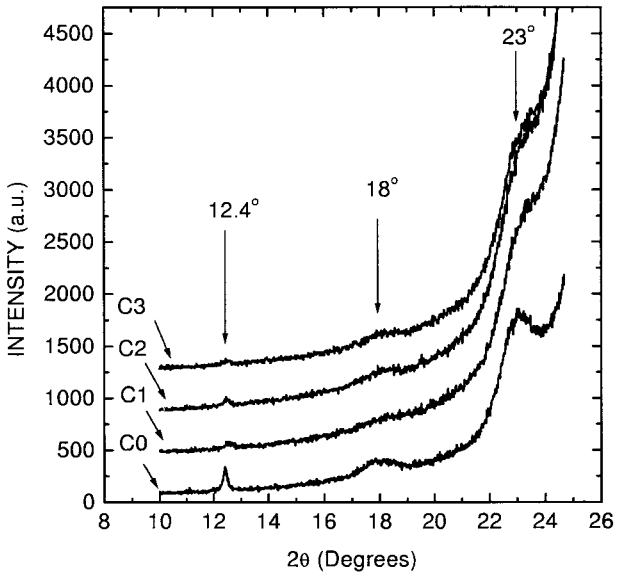

Figure 9 Low-angle portion of the X-ray diffractograms for a sequence of thermal cycles for a type A PET sample.

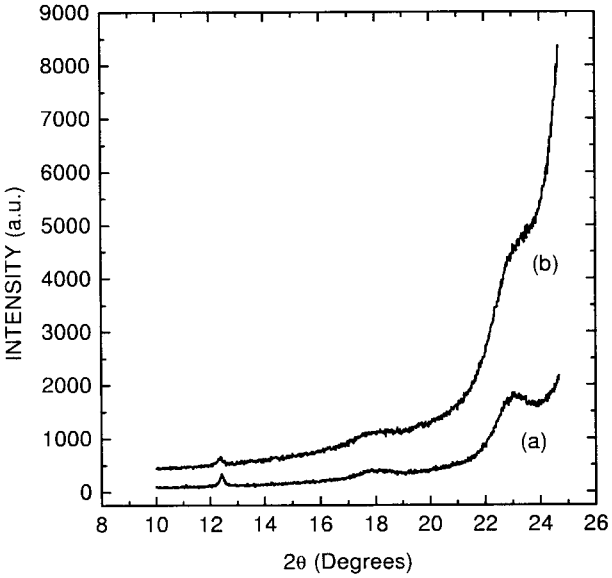

Figure 10 Low-angle X-ray diffractograms of uncycled type A (a) and type B (b) samples.

ple was subjected, is more clearly depicted in Figure 9 which exhibits the low-angle portion of the X-ray diffractograms for the entire sequence of thermally cycled samples are presented. In other words, the above X-ray diffraction data also validate the conclusion drawn from our photothermal measurements, that the effect of submitting our PET samples to thermal cycling above the crystalline glass-transition temperature is to enhance the sample amorphization.

Finally, to ensure that the proposed technique is indeed sensitive to the degree of sample crystallinity, we have repeated the photothermal measurements with type B PET samples. As mentioned earlier, type B samples were taken from a region with no apparent marks of the calendering process. Accordingly, we expected these samples to be less crystalline than type A samples. In fact, the comparison between the X-ray diffractograms of uncycled type A and type B samples indeed shows that type B samples are less crystalline than type A. This is clearly shown in Figure 10, which displays the low-angle diffractograms of these two samples. The thermal diffusivity data for type B samples, as determined by the photothermal measurements, is shown in Figure 11 as a function of temperature. The interesting point here is that the thermal diffusivity data remained practically unchanged upon subjecting the samples to thermal cycling. The actual data shown in Figure 11 corresponds to the average of data of the first and second cycling. We also note that the values of the thermal diffusivity started, near room temperature, at values close to the end values (between 80° and 90°C) of the thermal diffusivity of type A samples after the third cycling.

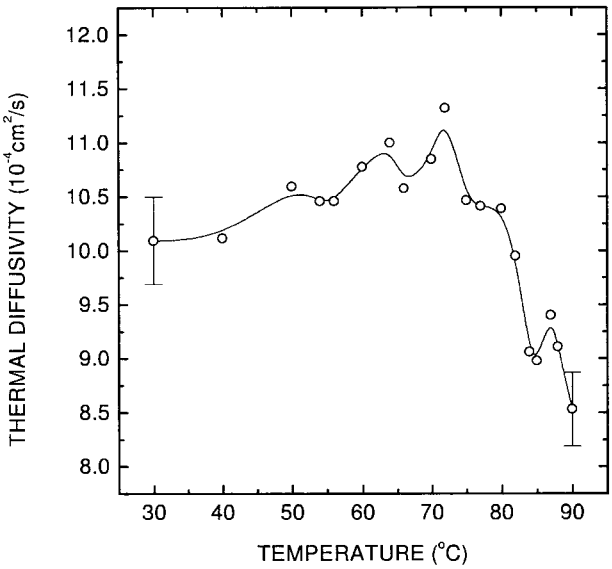

Figure 11 Thermal diffusivity of a type B sample as a function of temperature, as determined by the photothermal measurements. The data remained practically unchanged during the first two thermal cyclings.

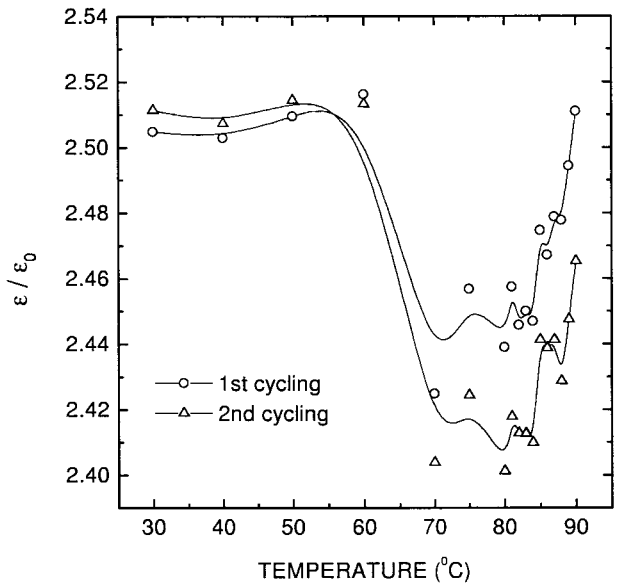

Figure 12 Dielectric constant as a function of temperature of a type B sample corresponding to the first (a) and second (b) thermal cycling.

Figure 11 also exhibits the two peaks at ~ 72°C and 86°C, corresponding to the glass-transition temperatures of the amorphous and crystalline fractions, respectively. The same tendency to exhibit lower values, as compared to those of type A samples, was also observed in the dielectric constant measurements of type B samples, as a function of temperature. These results are summarized in Figure 12. As in the case of the thermal diffusivity, the dielectric constant of type B samples remained also practically unchanged during the first and second thermal cycling. They also started, near room temperature, at a value that was lower than those of type A samples, and exhibited a broad minimum around 75°C. In other words, the same trends exhibited in the photothermal measurements of the thermal diffusivity were also manifested in the dielectric constant measurements thereby demonstrating that the former thermal characterization technique is, indeed, sensitive to changes in the crystalline fraction of the polymer.

CONCLUSIONS

This article discusses the use of piezo- and pyroelectric photothermal detection for measurements of thermal properties of polymers as a function of temperature as well as to monitor the changes induced by thermal aging. The proposed technique was tested using poly(ethylene terephthalate) samples with distinct degrees of crystallinity. For the more crystalline samples, the photothermal thermal diffusivity measurements were not only sensitive to the glass transitions characteristic of the amorphous and crystalline fractions of poly(ethylene terephthalate), but they also exhibited the marked effects of the sample thermal cycling. On subjecting the sample to repeated temperature cycling above the crystalline glass transition temperature the sample tends to enhance its amorphous fraction. This thermal aging effect was also manifested in the dielectric constant measurements and confirmed by X-ray diffraction on the thermally cycled samples. Furthermore, the proposed photothermal technique also provided qualitative information regarding the temperature behavior of the sample thermal expansion coefficient. The photothermal measurements also proved to be extremely sensitive to the sample's degree of crystallinity. This was clearly demonstrated by the difference between the thermal diffusivity values found for type A (more crystalline) and type B (more amorphous) samples.

We hope the suggested photothermal characterization technique will prove to be an important auxiliary tool in the polymer research area. For instance, with minor modifications, this technique can be adapted in a straightforward manner to monitoring kinetics processes, such as curing and sedimentation, as a function of temperature.

REFERENCES

1. Rosencwaig, A. Photoacoustics and Photoacoustic Spectroscopy; Wiley: New York, 1980.
2. Tam, A. C. Rev Mod Phys 1986, 58, 381.
3. Vargas, H.; Miranda, L. C. M. Phys Rep 1988, 161, 43.
4. Pessoa, O., Jr.; Cesar, C. L.; Patel, N. A.; Vargas, H.; Ghizoni, C. C.; Miranda, L. C. M. J Appl Phys 1986, 59, 1316.
5. Ghizoni, C. C.; Miranda, L. C. M. Phys Rev 1985, B32, 8392.
6. John, P. K.; Miranda, L. C. M.; Rastogi, A. Phys Rev 1986, B34, 4342.
7. Mansanares, A. M.; Baesso, M. L.; da Silva, E. C.; Gandra, F. C. G.; Vargas, H.; Miranda, L. C. M. Phys Rev 1989, B40, 7912.
8. Baesso, M. L.; Bento, A. C.; de Andrade, A. A.; Sampaio, J. A.; Pecoraro, E.; Nunes, L. A.; Catunda, T.; Gama, S. Phys Rev 1998, B57, 10545.

9. Fork, D. C.; Herbert, S. K. Photochem Photobiol 1993, 57, 207.
10. Silva, W. J.; Priolli, L. M.; Magalhaes, A. C. N.; Pereira, A. C.; Vargas, H.; Mansanares, A. M.; Cella, N.; Miranda, L. C. M.; Alvarado-Gil, J. J. Plant Sci 1995, 104, 177.
11. Lachaine, A.; Poulet, P. Appl Phys Lett 1984, 45, 953.
12. Leite, N. F.; Cella, N.; Vargas, H.; Miranda, L. C. M. J Appl Phys 1987, 61, 3023.
13. Torres-Filho, A.; Perondi, L. F.; Miranda, L. C. M. J Appl Polym Sci 1988, 35, 103.
14. Dadarlat, D.; Bicazan, M.; Frandas, A.; Morariu, V. V.; Pasca, A.; Jalink, H.; Bicanic, D. Instrum Sci Technol 1997, 25, 235.
15. Merté, B.; Korpiun, P.; Lüsher, E.; Tilgner, R. J Phys Coll 1983, 44, 463.
16. Korpiun, P.; Merté, B.; Fritsch, G.; Tilgner, R.; Lüsher, E. Coll Polym Sci 1983, 261, 312.
17. Franzan, A. H.; Leite, N. F.; Miranda, L. C. M. Appl Phys 1990, A50, 431.
18. Bandrup, J.; Immergut, E. H., Eds. Polymer Handbook, 3rd Ed.; Wiley: New York, 1989.
19. Coufal, H. J Vac Sci Technol 1987, A5, 2875.
20. Jackson, W.; Amer, N. M. J Appl Phys 1980, 51, 3343.
21. Bass, M., Ed. Handbook of Optics. Vol. II; McGraw-Hill: New York, 1995.
22. Elias, H. G. Macromolecules: Structure and Properties; Plenum: New York, 1984.